Table 2. *Average bond valences and bond-valence sums for* $Ta_4P_4S_{29}$

The number preceeding the atom symbol is the number of atoms in the formula unit, and the entries in the table are the numbers of bonds per formula unit and their average valence. The last column is the bond-valence sum for the atoms in the left column.

	4Ta	4P	16S	8S′	5S″	Sum
4Ta	–	–	16 × 0.73	16 × 0.63	–	4 × 5.46
4P	–	–	16 × 1.23	–	–	4 × 4.95
16S	16 × 0.73	16 × 1.23	–	–	–	16 × 1.97
8S′	16 × 0.63	–	–	8 × 1.06	–	8 × 2.33
5S″	–	–	–	–	10 × 1.02	5 × 2.04

Table 3. *Average bond valences and bond-valence sums for* $FePS_3$

The entries in the table have the same significance as for Table 2.

	Fe	P	3S	Sum
Fe	–	–	6 × 0.35	2.09
P	–	1.00	3 × 1.24	4.72
3S	6 × 0.35	3 × 1.24	–	3 × 1.98

A simple example of a case where 'cation'–'cation' bonding *is* unambiguous is afforded by the structure of $FePS_3$ (Klingen, Eulenberger & Hahn, 1973). In this structure P_2 groups center octahedra of S atoms and act as 'cations' with each P atom bonded to one P and three S atoms. This interpretation of the structure is supported by the bond valences [again calculated from equation (1) using the observed bond lengths] reported in Table 3. The P—P bond has a valence of 1.0; the bond-valence sums have the values expected for Fe octahedrally coordinated by S (2) and for P acting as a cation (5) and for S acting as an anion (2).

RZERO is available from the authors as a subroutine written in ANSI standard FORTRAN77.

This work was supported by a grant (DMR 8813524) from the National Science Foundation. NEB gratefully acknowledges support from a National Science Foundation Fellowship.

References

BRESE, N. E. & O'KEEFFE, M. (1991). *Acta Cryst.* **B47**, 192–197.
BROWN, I. D. (1981). *Structure and Bonding in Crystals*, Vol. II, edited by M. O'KEEFFE & A. NAVROTSKY, pp. 1–30. New York: Academic Press.
BROWN, I. D. & ALTERMATT, D. (1985). *Acta Cryst.* **B41**, 244–247.
EVIAN, M., QUEIGNEC, M., BREC, J. & ROUXEL, J. (1985). *J. Solid State Chem.* **56**, 148–157.
HULLIGER, F. (1981). *Structure and Bonding in Crystals*, Vol. II, edited by M. O'KEEFFE & A. NAVROTSKY, pp. 297–352. New York: Academic Press.
KLINGEN, W., EULENBERGER, G. & HAHN, H. (1973). *Z. Anorg. Allg. Chem.* **401**, 97–112.
O'KEEFFE, M. (1989). *Struct. Bonding (Berlin)*, **71**, 161–190.
O'KEEFFE, M. (1990). *Acta Cryst.* **A46**, 138–142.
O'KEEFFE, M. & BRESE, N. E. (1991). *J. Am. Chem. Soc.* **113**, 3226–3229.
WELLS, A. F. (1984). *Structural Inorganic Chemistry*, 5th ed. Oxford: Clarendon Press.

Acta Cryst. (1992). **B48**, 154–160

Deformation Density in Lithium Triborate, LiB_3O_5

BY S. F. RADAEV, B. A. MAXIMOV AND V. I. SIMONOV

Institute of Crystallography, Academy of Sciences of Russia, Leninsky pr. 59, 117333 *Moscow, Russia*

B. V. ANDREEV

Institute of Physical Chemistry, Academy of Sciences of Russia, Leninsky pr. 31, 117915 *Moscow, Russia*

AND V. A. D'YAKOV

Physical Faculty, Moscow State University, 117234 *Moscow, Russia*

(*Received* 8 *May* 1991; *accepted* 8 *November* 1991)

Abstract

An accurate set of X-ray data collected at 293 K was used to refine the structure and study the deformation density of the title compound, LiB_3O_5. M_r = 119.371, orthorhombic, $Pna2_1$, a = 8.447 (1), b = 7.3789 (8), c = 5.1408 (6) Å, V = 320.4 (1) Å^3, Z = 4, D_x = 2.47 g cm^{-3}, μ = 2.5 cm^{-1}, λ(Mo $K\alpha$) = 0.71076 Å, $F(000)$ = 232, R = 0.0188, wR = 0.0190 for 1130 reflections ($s > 0.4$ Å^{-1}). According to the deformation electron density distribution, the vacant $2p$ orbital of the triangularly coordinated B(1) atom is mainly populated by electrons belonging to lone pairs of the O(1) and O(2) atoms which are linked by

0108-7681/92/020154-07$03.00

short bonds to the B(1) atom. The vacant $2p$ orbital of the B(3) atom is also triangularly coordinated and is mainly populated by electrons from a lone pair of a single oxygen O(4) atom. From the analysis of the atomic arrangement of LiB_3O_5, it is possible that a highly anisotropic Li-ion conductivity exists in the title compound.

Introduction

In recent years there has been a growing interest in lithium borates. The reason is that these compounds possess a unique combination of nonlinear-optical, acousto-optical and physical properties which promise a wide variety of practical applications. Single crystals have been studied by X-ray diffraction techniques (Shevyrev, Muradyan, Simonov, Egorov-Tismenko, Simonov & Belov, 1981; Kirfel, Will & Stewart, 1983; Radaev, Muradyan, Malakhova, Burak & Simonov, 1989). Lithium triborate, LiB_3O_5 (LBO), the excellent nonlinear-optical characteristics of which have aroused great attention, is of special interest. It has been shown (Lin, Sun, Wu & Chen, 1990) that LBO is especially advantageous in frequency conversion of high-power pulse lasers. It is expected that LBO will be widely and effectively used in harmonic and sum-frequency generation (with Nd:YAG and dye lasers), optical parametric oscillation and laser fusion. It should also be noted that the possible application of nonlinear-optical materials in laser systems for thermonuclear fusion experiments imposes additional requirements, in particular, radiation stability. Our preliminary investigations have shown that LBO meets the latter requirement, in contrast to such well-known materials as KH_2PO_4 (KDP), $LiNbO_3$ (LN), $Ba_2NaNb_5O_{15}$ (BNN) and $KTiOPO_4$ (KTP). For example, at room temperature stable colour centres were not formed within the whole transparency range of LBO under irradiation by fast electrons with $E_e = 5.5$ MeV up to an absorbed dose of 10^8 Gy.

So far only one structural study of LiB_3O_5 has been carried out, *i.e.* by the photomethod using a Guinier chamber (Konig & Hoppe, 1978).

Experimental

LiB_3O_5 single crystals were grown from solution in the melt. Crystallization was carried out using oriented seeds and an excess of boron oxide relative to the stoichiometric composition. The temperature was gradually decreased and the growth rate was controlled. The diffraction data were collected on an Enraf–Nonius CAD-4 diffractometer. The lattice constants were refined by least-squares methods from 20 reflections with $14 < \theta < 28°$. The experimental data are listed in Table 1.

Table 1. *Experimental and refinement details*

Radiation	Mo $K\alpha$
Wavelength (Å)	0.71076
Monochromator	Graphite
Temperature (K)	293
Crystal habit	Sphere
Diameter (mm)	0.320
Space group	$Pna2_1$
a (Å)	8.447 (1)
b (Å)	7.3789 (8)
c (Å)	5.1408 (6)
hkl range	$-16 \le h \le 16$, $-14 \le k \le 14$, $-10 \le l \le 10$
Scan mode	$\theta - \frac{1}{3}\theta$ step scan*
Scan width (°)	$0.8 + 0.35\tan\theta$
Intensity standards	One
Decomposition (%)	< 2
Reflections measured	8989
Observed reflections $[I > 3\sigma(I)]$	8586
Agreement factor on I	0.036
Reflections used	1130†
$(\sin\theta/\lambda)_{max}$ (Å^{-1})	1.00
Linear absorption coefficient (cm^{-1})	2.5
g‡	2.66×10^{-4}
Weight	$[\sigma(F_o)]^{-2}$§
R	0.0188†
wR	0.0190†
GoF	2.02†

* The ratio between rotation angle of the sample and the rotation angle of the detector is fixed as 1/3 during measurements.

† High-order refinement [$(\sin\theta/\lambda) > 0.4$ Å^{-1}].

‡ Isotropic extinction correction, Becker & Coppens formalism, type-I Lorentzian distribution.

§ There are 96 steps in the scan interval. $\sigma(F_o)$ calculated from counting statistics.

No correction for absorption was made, $\mu R = 0.04$. The small corrections for anomalous dispersion, in particular $\Delta f''$, prevented a reliable determination of the absolute configuration of the structure. Therefore, all Friedel pairs were averaged, and the $\Delta f''$ corrections were neglected in the calculation of structure factors. Scattering curves of neutral atoms were taken from *International Tables for X-ray Crystallography* (1974, Vol. IV). All calculations were carried out using the program *PROMETHEUS* (Zucker, Perenthaler, Kuhs, Bachman & Shulz, 1983).

Structure refinement of LiB_3O_5

The initial model used for refinement of the LiB_3O_5 structure was that suggested by Konig & Hoppe (1978). Refinement, using the full data set of 1229 reflections, led to R factors $wR = 0.0200$, $R = 0.0204$ and GoF = 2.46. In order to choose the correct cut-off angle for a high-angle refinement, a series of independent refinements was carried out (the extinction parameter was fixed at the value obtained from the all-data refinement) using different $s = (\sin\theta/\lambda)_{min}$ values in steps of 0.05 Å^{-1} up to 0.75 Å^{-1}. A further reduction of the high-angle region was not considered, since the ratio of the number of independent

Table 2. *Fractional atomic coordinates and equivalent isotropic thermal parameters* ($Å^2$) *with e.s.d.'s in parentheses*

$$B_{eq} = (4/3)\Sigma_i\Sigma_j \beta_{ij} \mathbf{a}_i.\mathbf{a}_j.$$

	x	y	z	B_{eq}
Li	0.0873 (2)	0.0667 (2)	0.9548 (4)	1.50 (2)
B(1)	0.00968 (7)	0.66439 (8)	0.8098 (2)	0.552 (7)
B(2)	0.19437 (7)	0.44327 (8)	0.0063 (2)	0.469 (7)
B(3)	0.15705 (7)	0.74859 (8)	0.1895 (2)	0.504 (7)
O(1)	0.08644 (6)	0.50430 (6)	0.8022 (1)	0.670 (5)
O(2)	0.11633 (6)	0.29510 (6)	0.1535 (1)	0.605 (5)
O(3)	0.05809 (6)	0.79816 (6)	0.9848 (1)	0.653 (5)
O(4)	0.26102 (6)	0.09024 (6)	0.6902 (1)	0.519 (5)
O(5)	0.83898 (6)	0.12504 (6)	0.8840*	0.603 (5)

*The origin in space group $Pna2_1$ is fixed by this value.

reflections to the number of refined parameters was smaller than 8. Analysis of the dependence of the scaling factor, and of the atomic isotropic temperature factors on the cut-off angle revealed two regions: $s_1 = 0.35$–0.45 and $s_2 = 0.60$–0.70 $Å^{-1}$, where the refined parameters were rather stable. LiB_3O_5 contains only light atoms and scattering beyond $\sin\theta/\lambda = 0.4$ $Å^{-1}$ for the Li and B atoms is almost fully determined by their $1s^2$ electrons. For the O atoms the value of this scattering is not less than 80% of the total oxygen scattering. Analyses of electron density distribution maps for $s = 0.6$ $Å^{-1}$ showed that they neither differed qualitatively nor bore additional information compared to $s = 0.4$ $Å^{-1}$, while the error level increased considerably. In addition, for $s = 0.6$ $Å^{-1}$ the correlation between refined parameters was more significant. *e.g.* correlation coefficients between the scaling factor and the atomic temperature factors are 0.72 for $s = 0.6$ $Å^{-1}$ and 0.50 for $s = 0.4$ $Å^{-1}$. Therefore $s = 0.4$ $Å^{-1}$ was chosen as the cut-off angle for the high-angle refinement. Atomic parameters and interatomic distances taken from the high-angle refinement are listed in Tables 2, 3 and 4.*

The B atoms are located within coordination polyhedra of two types, triangles and tetrahedra, which are characteristic of this element. Fig. 1(*a*) shows a projection of the LiB_3O_5 structure onto the (001) plane. The B(1) and B(3) atoms lie within the planar triangles formed by the O(1), O(2), O(3) and O(3), O(4), O(5) atoms, respectively. The presence of two slightly different short bonds and one longer bond is a specific feature of these arrangements. The largest O(1)—B(1)—O(2) and O(4)—B(3)—O(5) valence angles in the triangles are 123.32 and 124.92°, respectively, which are formed by the short

Table 3. *Interatomic distances* (Å) *and angles* (°) *with e.s.d.'s in parentheses*

B(1)—O(1)	1.3481 (8)	B(3)—O(3)^{ii}	1.3930 (8)
B(1)—O(2)^{i}	1.3666 (8)	B(3)—O(4)^{iii}	1.3581 (8)
B(1)—O(3)	1.3967 (8)	B(3)—O(5)^{v}	1.3675 (8)
B(2)—O(1)^{ii}	1.4610 (8)	Li—O(2)^{vi}	1.986 (2)
B(2)—O(2)	1.4843 (8)	Li—O(3)^{vii}	2.003 (2)
B(2)—O(4)^{iii}	1.4872 (8)	Li—O(4)	2.009 (2)
B(2)—O(5)^{iv}	1.4633 (8)	Li—O(5)^{viii}	2.172 (2)

O(1)—B(1)—O(2)^{i}	123.32 (5)	O(3)^{ii}—B(3)—O(4)^{iii}	122.24 (5)
O(1)—B(1)—O(3)	119.81 (5)	O(3)^{ii}—B(3)—O(5)^{v}	112.84 (5)
O(2)^{i}—B(1)—O(3)	116.87 (5)	O(4)^{iii}—B(3)—O(5)^{v}	124.92 (5)
O(1)^{ii}—B(2)—O(2)	108.43 (5)	O(2)^{vi}—Li—O(3)^{vii}	144.6 (1)
O(1)^{ii}—B(2)—O(4)^{iii}	112.94 (5)	O(2)^{vi}—Li—O(4)	100.7 (1)
O(1)^{ii}—B(2)—O(5)^{iv}	108.58 (5)	O(2)^{vi}—Li—O(5)^{viii}	92.1 (1)
O(2)—B(2)—O(4)^{iii}	109.00 (5)	O(3)^{vii}—Li—O(4)	103.2 (1)
O(2)—B(2)—O(5)^{iv}	109.64 (5)	O(3)^{vii}—Li—O(5)^{viii}	95.2 (1)
O(4)^{iii}—B(2)—O(5)^{iv}	108.23 (5)	O(4)—Li—O(5)^{viii}	125.1 (1)

Symmetry codes: (i) $-x, 1-y, \frac{1}{2}+z$; (ii) $x, y, -1+z$; (iii) $\frac{1}{2}-x, \frac{1}{2}+y, -\frac{1}{2}+z$; (iv) $-\frac{1}{2}+x, \frac{1}{2}-y, -1+z$; (v) $1-x, 1-y, -\frac{1}{2}+z$; (vi) $x, y, 1+z$; (vii) $x, -1+y, z$; (viii) $-1+x, y, z$.

Table 4. *Thermal motion ellipsoids*

φ_a, φ_b, φ_c are angles between main axes of thermal motion ellipsoids and coordinate axis (°); e.s.d.'s for angles are accurate to the last digit.

	R.m.s. amplitude (Å)	φ_a	φ_b	φ_c
Li	0.100 (3)	86	10	81
	0.124 (2)	46	86	136
	0.178 (2)	44	99	47
B(1)	0.075 (1)	53	89	37
	0.079 (1)	86	175	92
	0.095 (1)	142	95	53
B(2)	0.068 (1)	103	41	52
	0.079 (1)	152	115	79
	0.083 (1)	66	120	41
B(3)	0.069 (1)	79	33	59
	0.079 (1)	156	70	102
	0.090 (1)	110	115	34
O(1)	0.074 (1)	60	76	34
	0.078 (1)	63	153	91
	0.118 (1)	138	113	56
O(2)	0.072 (1)	136	104	49
	0.077 (1)	80	166	100
	0.109 (1)	48	91	42
O(3)	0.073 (1)	53	79	39
	0.075 (1)	75	165	88
	0.118 (1)	139	100	51
O(4)	0.062 (1)	86	31	59
	0.077 (1)	36	75	122
	0.100 (1)	54	117	48
O(5)	0.060 (1)	109	136	52
	0.078 (1)	155	65	90
	0.115 (1)	75	56	38

bonds. The smallest O(2)—B(1)—O(3) and O(3)—B(3)—O(5) angles are 116.87 and 112.84°. It should be noted that the O(3)—O(5) edge in the B(3) triangle has a minimum length of 2.299 Å as compared with the other O—O distances. The coordination polyhedron of the third independent boron atom B(2) is a tetrahedron. The two B(2)—O(1) and B(2)—O(5) bonds in this tetrahedron are short (1.4610 and 1.4633 Å), while the other two – B(2)—O(2) and B(2)—O(4) – are long (1.4843 and

* Lists of structure factors and anisotropic thermal parameters have been deposited with the British Library Document Supply Centre as Supplementary Publication No. SUP 54692 (21 pp.). Copies may be obtained through The Technical Editor, International Union of Crystallography, 5 Abbey Square, Chester CH1 2HU, England.

1.4872 Å). The valence angles, except O(1)—B(2)—O(4) which is 112.94°, are close to 109.5°, typical of an ideal tetrahedron.

The main structural unit of the LiB_3O_5 structure consists of two B triangles and one B tetrahedron (Fig. 1). The triangles possess a common vertex, the O(3) atom. In addition, each is linked to a B(2) tetrahedron *via* O(1) and O(4), respectively. The structural units, linked to form chains along [001] are related by the 2_1 axis (Fig. 1*b*). Adjacent chains are joined *via* O(5) oxygen atoms belonging to both a B(2) tetrahedron and a B(3) triangle. The structure is cemented by Li atoms located in the framework voids. These voids form continuous channels parallel to *c*. The first coordination sphere of the Li atom contains four oxygen atoms, O(2), O(3), O(4) and O(5), which form a distorted tetrahedron. Three bonds in this tetrahedron – Li—O(2) (1.986 Å), Li—O(3) (2.003 Å) and Li—O(4) (2.009 Å) – are approximately equal in length, whereas the fourth bond, Li—O(5), is significantly longer (2.172 Å). Thus, the Li atom is displaced from the tetrahedron center towards the O(2), O(3), O(4) face (the distance between Li and the face is 0.36 Å). The specific arrangement of the O(3)—Li and O(5)—Li^{i} bonds [symmetry code: (i) $-x, -y, \frac{1}{2}+z$] (Fig. 1*a*) apparently accounts for a shortened O(3)—O(5) distance in the B(3) triangle, as mentioned above. Other oxygen atoms lie at distances of at least 2.696 Å from the Li atom. In terms of their coordination, the O(1), O(2), O(4) and O(5) atoms can be divided into two pairs: O(1), O(5) and O(2), O(4). Each of the O(1) and O(5) atoms is linked to boron atoms in triangular and tetrahedral coordination by short bonds, and either does not have [this refers to O(1)] or has a long [O(5) atom] bond with Li atoms. As for the O(2), O(4) pair, each oxygen atom is linked by a short bond to a B atom in triangular coordination, by a long bond to a B atom in tetrahedral coordination, and has short bonds to the Li atoms. The O(3) atom is linked by two long bonds to B atoms in triangular coordination and has a short bond with the Li atom.

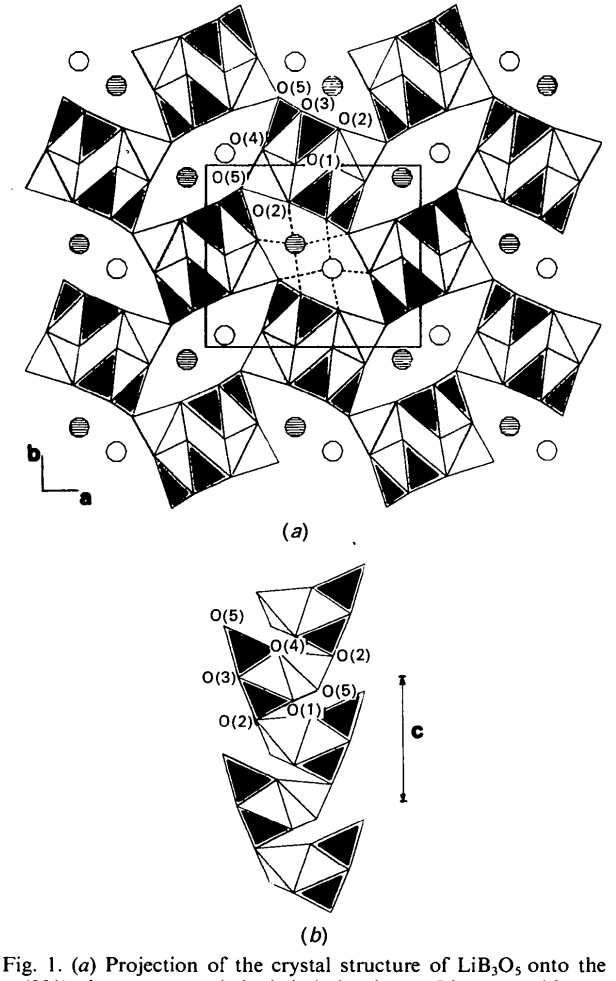

Fig. 1. (*a*) Projection of the crystal structure of LiB_3O_5 onto the (001) plane; open and shaded circles denote Li atoms with z = 0.9548 and 0.4548, respectively. (*b*) Structure fragment illustrating the junction of structural units.

Deformation density

Deformation electron density sections which elucidate the chemical bonding in lithium triborate are shown in Figs. 2–5. To form bonds with three oxygen atoms each B(1) and B(3) atom uses its sp^2 hybrid orbitals with three valence electrons. The geometries of the B(1) and B(3) triangles have very much in common, and their electron density distributions exhibit similar features. The highest peaks in the B(1) triangle (0.33 and 0.27 e Å^{-3}) are observed for the short B(1)—O(1) and B(1)—O(2) bonds, while the deformation density peak height on the long B(1)—O(3) bond is lower – 0.23 e Å^{-3} (Fig. 2*a*). The maximum background in the difference density maps does not exceed 0.07 e Å^{-3}. Similar findings are observed for the B(3) triangle: the deformation density peaks on the short B(3)—O(4) and B(3)—O(5) bonds are 0.34 and 0.30 e Å^{-3}, respectively, while the peak on the B(3)—O(3) bond is much lower – 0.22 e Å^{-3} (Fig. 3*a*). The shapes of the deformation density peaks on the shortest B(1)—O(1) and B(1)—O(2) bonds in the B(1) triangle indicate that a pure σ-type bond is not realized in these two cases. This is supported by elongated peaks perpendicular to the plane of the triangle (Figs. 2*b* and 2*c*). In contrast to this, the peak on the long B(1)—O(3) bond is extended along the bond, is symmetrical with respect to it (Fig. 2*d*), and indicates a predominantly σ-type bond. The vacant 2*p* orbital of the B(1) atom may serve as a basis for a common orbital being partially populated by lone-pair electrons belonging to the

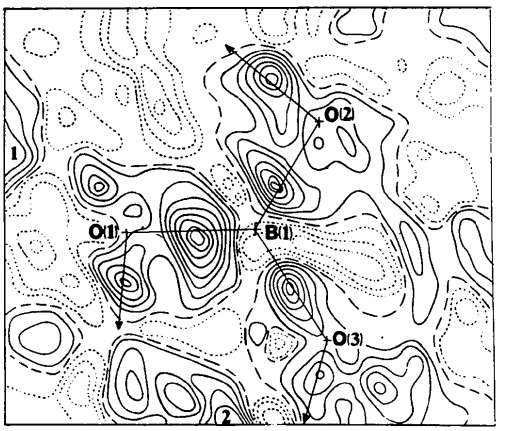

(*a*)

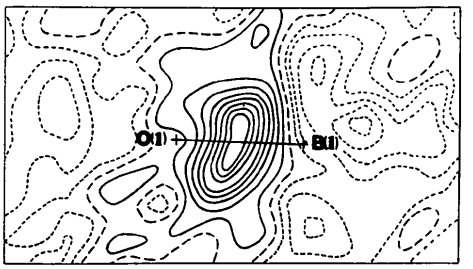

(*b*)

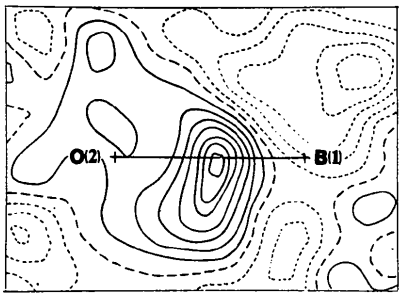

(*c*)

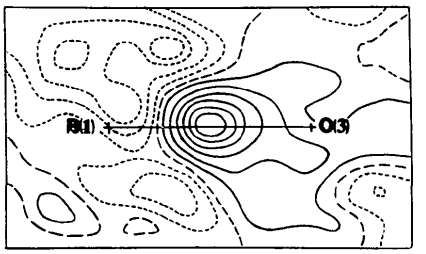

(*d*)

Fig. 2. Deformation electron densities in the plane of O(1), O(2), O(3) (*a*), along three B(1)—O bonds and perpendicular to the O(1), O(2), O(3) plane (*b*)–(*d*). Directions towards nearest B atoms are indicated by arrows. Contours at 0.04 e $Å^{-3}$; negative contours are dotted, zero line broken. Numbers in (*a*) denote: (1) a trace of the lone electron pair of the O(1) atom from an adjacent structural unit; (2) a trace of the peak on the B(3)—O(4) bond; a trace of the peak on the O(4)—B(2) bond is seen to the left.

O(1) and O(2) atoms. Deformation density peaks extended perpendicular to the directions of these two bonds are presumably due to overlap of the σ-bond electrons and the above lone-pair electrons. The electron density distribution in the B(3) triangle differs slightly from the one discussed above. In a

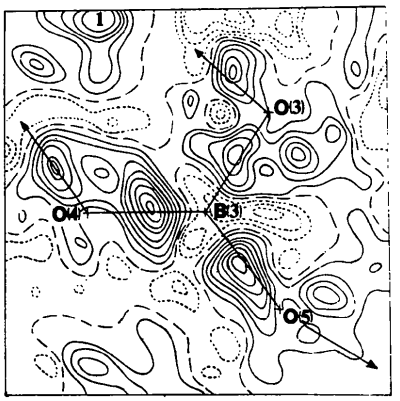

(*a*)

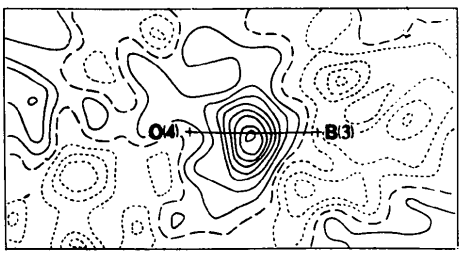

(*b*)

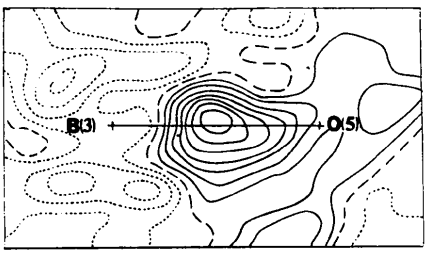

(*c*)

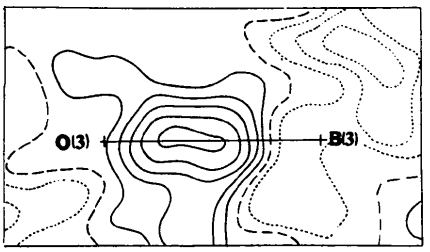

(*d*)

Fig. 3. Deformation electron densities in the plane of O(3), O(4), O(5) (*a*), along three B(3)—O bonds and perpendicular to the O(3), O(4), O(5) plane (*b*)–(*d*). Symbols and contours are as in Fig. 2. Numbers in (*a*) denote: (1) a trace of the peak on the B(1)—O(1) bond.

similar manner to the B(1) triangle, the deformation density peak located on the short B(3)—O(4) bond is noticeably extended along the direction perpendicular to the B(3) triangle (Fig. 3*b*). However, in contrast to the B(1) triangle, the deformation density peak on the second short bond, B(3)—O(5), is not extended along the direction perpendicular to the plane of the B(3) triangle (Fig. 3*c*). This indicates a predominance of σ-type bonding in this particular case. The peak located on the longest B(3)—O(3) bond is extended along it, being rather symmetrical relative to the bond direction (Fig. 3*d*). Therefore, there must be almost pure σ-type bonding. Thus, lone-pair electrons of the O(4) atom are responsible for the population of the vacant $2p$ orbital of the B(3) atom. In addition to the deformation electron density corresponding to the O—B(1) and O—B(3) bonds, Figs. 2(*a*) and 3(*a*) also show traces of deformation density peaks on the O—B(2) bonds.

Two sections showing bonding in the B(2) tetrahedron are presented in Fig. 4. All the B(2)—O bonds exhibit deformation electron density peaks, of 0.14–0.32 e $Å^{-3}$. The B(2) atom lends its four sp^3 hybrid orbitals to the formation of bonds with the O atoms. The highest peaks of 0.32 and 0.28 e $Å^{-3}$ are located on the long B(2)—O(2) and B(2)—O(4) bonds. On the short B(2)—O(1) and B(2)—O(5) bonds, the deformation density peak heights are much lower – 0.21 and 0.14 e $Å^{-3}$, respectively. Besides the above peaks, the B—O bonds exhibit deformation density peaks near each oxygen atom, which can be interpreted as oxygen lone pairs. These peaks are located at distances of 0.52–0.64 Å from the O atoms, being 0.16–0.23 e $Å^{-3}$ in height. Traces of some of these peaks are seen in Figs. 2(*a*) and 3(*a*).

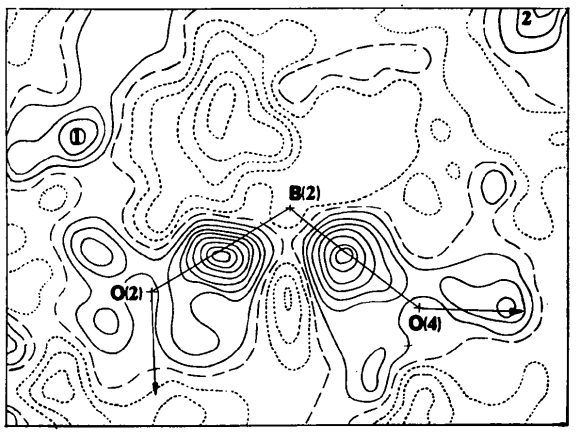

(*a*)

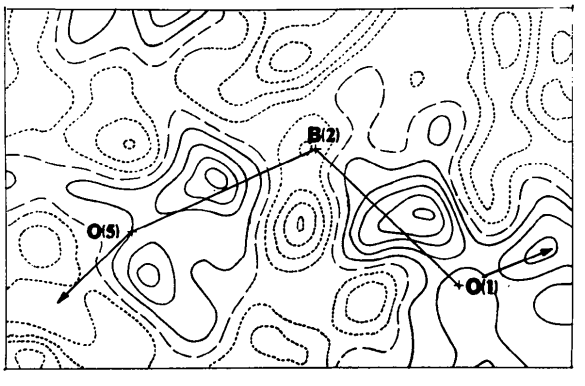

(*b*)

Fig. 4. Deformation electron densities in the planes of O(2), B(2), O(4) (*a*) and O(1), B(2), O(5) (*b*). Symbols and contours are as in Fig. 2. Numbers in (*a*) denote: (1) a trace of the lone electron pair of the O(5) atom; (2) a trace of the lone electron pair of the O(2) atom.

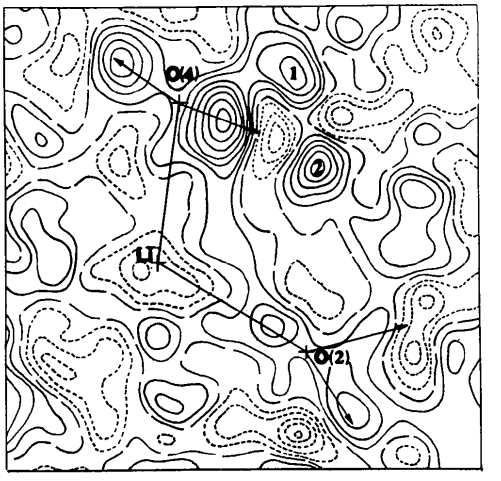

(*a*)

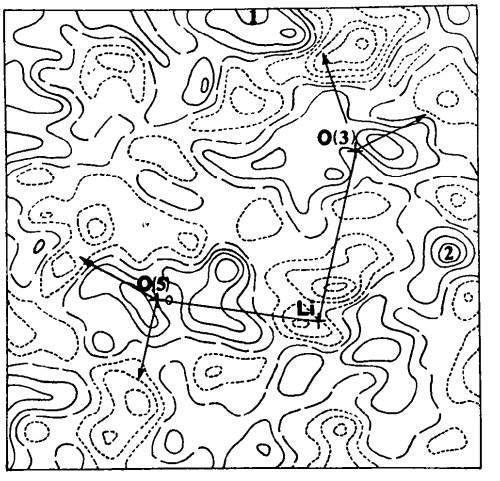

(*b*)

Fig. 5. Deformation electron densities in the planes of O(2), Li, O(4) (*a*) and O(3), Li, O(5) (*b*). Symbols and contours are as in Fig. 2. Numbers in (*a*) denote: (1) a trace of the peak on the B(3)—O(3) bond; (2) a trace of the peak on the B(3)—O(5) bond. Numbers in (*b*) denote: (1) a trace of the peak on the B(1)—O(2) bond; (2) a trace of the lone electron pair of the O(4) atom.

The ionic character of the bonding in the Li tetrahedra is confirmed by the absence of electron density peaks in the Li—O bond directions. Fig. 5 shows two deformation electron density sections illustrating the Li—O bonds. One can clearly see 'lone-pair' regions of O(2)—O(5) atoms oriented towards the Li atom. This type of electron density distribution is quite common in an Li coordination polyhedron as reported, for example, by Shevyrev *et al.* (1981) and Kirfel *et al.* (1983).

Concluding remarks

Our results provide refined parameters of the structure of LiB_3O_5. Some Li—O and B—O distances differ from the results given by Konig & Hoppe (1978), by values which exceed the standard deviations by more than an order of magnitude. The presence of channels passing throughout the structure, parallel to *c*, and containing Li atoms suggests a possible ionic conductivity in this direction. Ionic conductivity in the directions perpendicular to *c* is hardly probable. All the B—O—B angles in the structures can be considered as close to 120°. One can then suppose that the electron deficiency in the B tetrahedra of the lithium triborate structure results in the formation of a delocalized orbital involving the entire boron–oxygen framework. This orbital can be roughly described as a sum of three-center orbitals forming the B—O—B bridges, the angle containing the O atom being equal to 120°. A similar situation has been reported previously by Shevyrev *et al.* (1981) and Lipscomb (1973). The authors of an earlier work (Davydov, Derkacheva, Dunina, Zhabotinskii, Zolin, Koreneva & Samokhina, 1970) assumed that the presence of delocalized multicentred valence orbitals accounts for the high nonlinear susceptibility in the crystals. It should also be noted that our results agree with the conclusions of the so-called theory of anionic groups for nonlinear-optical susceptibility in crystals (Chen & Liu, 1986). According to this theory, the larger the distortions in oxygen polyhedra or any other anionic groups of a structure, and the more inhomogeneous the electron deformation density distribution on the bonds in these groups, the higher are the values of the second-order microscopic susceptibility. As one can conclude from Chen, Wu & Li (1990), in the case of LBO the experimental data agree with the theoretical assumptions. Our structural data allow much more accurate calculations to be carried out in future work.

References

Chen, C. & Liu, G. (1986). *Annu. Rev. Mater. Sci.* **16**, 203–243.

Chen, C., Wu, Y. & Li, R. (1990). *J. Cryst. Growth*, **99**, 790–798.

Davydov, B. L., Derkacheva, L. D., Dunina, V. V., Zhabotinskii, M. E., Zolin, V. F., Koreneva, L. G. & Samokhina, M. A. (1970). *Pisma Zh. Eksp. Teor. Fiz.* **12**, 24–26.

Kirfel, A., Will, G. & Stewart, R. F. (1983). *Acta Cryst.* B**39**, 175–185.

Konig, H. & Hoppe, R. (1978). *Z. Anorg. Allg. Chem.* **439**, 71–79.

Lin, S., Sun, Z., Wu, B. & Chen, C. (1990). *J. Appl. Phys.* **67**, 634–638.

Lipscomb, W. N. (1973). *Acc. Chem. Res.* **6**(8), 257–269.

Radaev, S. F., Muradyan, L. A., Malakhova, L. F., Burak, Ya. V. & Simonov, V. I. (1989). *Sov. Phys. Crystallogr.* **34**(6), 842–846.

Shevyrev, A. A., Muradyan, L. A., Simonov, V. I., Egorov-Tismenko, Yu. K., Simonov, M. A. & Belov, N. V. (1981). *Dokl. Akad. Nauk SSSR*, **257**(1), 111–114.

Zucker, U. H., Perenthaler, E., Kuhs, W. F., Bachman, R. & Shulz, H. (1983). *J. Appl. Cryst.* **16**(3), 358.

Acta Cryst. (1992). B**48**, 160–166

Phase Transition in Rubidium Nitrate at 346 K and Structure at 296, 372, 413 and 437 K

By Jutta Pohl, Dieter Pohl and Gunadi Adiwidjaja

Mineralogisch-Petrographisches Institut der Universität Hamburg, Grindelallee 48, *D*-2000 *Hamburg* 13, *Germany*

(*Received* 22 *May* 1991; *accepted* 11 *November* 1991)

Abstract

Rubidium nitrate, $RbNO_3$, $M_r = 147.474$, trigonal, space group $P3_1$ for both structures: below the irreversible first-order phase transition at 346 K and above. Another crystal exhibited space group $P3_2$. Crystal growth from aqueous solution at 290 K. At 296 K: $a = 10.474$ (1), $c = 7.443$ (1) Å, $V = 707.2$ (2) Å^3, $D_x = 3.116$ (1) g cm^{-3}, refractive indices $n_\omega = 1.5250$ (1) and $n_\varepsilon = 1.5267$ (3). After

0108-7681/92/020160-07$03.00